Hysteretic Three-State Redox Interconversion among Zigzag Bisquinodimethanes with Non-fused Benzene Rings and Twisted Tetra-/Dications with [5]/[3]Acenes Exhibiting NIR Absorptions

Yusuke Ishigaki,* Takashi Harimoto, Kazuma Sugawara, Takanori Suzuki*

Department of Chemistry, Faculty of Science, Hokkaido University, Sapporo 060-0810, Japan

KEYWORDS: redox system, acene, three-state switching, near-infrared absorption, charge-transfer interaction

ABSTRACT: Octaaryl-substituted bisquinodimethanes (BQDs) with a zigzag structure were designed as redox switchable molecules that undergo four-electron oxidation to produce tetracationic pentacenes with a doubly twisted structure. In contrast to one-stage four-electron oxidation of BQDs, stepwise two-electron reduction of tetracationic pentacenes occurs to give dicationic anthracenes and then the original BQDs, step-by-step. Since both tetra-/dications exhibit near-infrared (NIR) absorptions (-1,400 nm) based on an intramolecular charge-transfer interaction, changes in not only their structures but also UV–vis–NIR spectra can be controlled by redox stimuli. In this paper, we present an unprecedented one-step π-extension to pentacene from non-fused benzene rings by oxidation, and subsequent two-stage deannulation to benzene rings via anthracene upon reduction; all structures were determined by single-crystal X-ray analyses and their properties were characterized by spectroscopic and theoretical studies.

[*n*]Acenes are a class of aromatic hydrocarbons composed of linearly fused benzene rings (e.g., anthracene, tetracene, pentacene, etc.; *n*: number of annulated benzene rings). [*n*]Acenes are highly attractive molecules because their HOMO/LUMO levels and small band gap can be easily modulated by π-extension and the introduction of various substituents or steric strain to the acene core.[1–11] Thus, their optical and electrochemical properties can be fine-tuned. As a result, [*n*]acenes are widely used as functional organic materials such as semiconductors,[12–15] fluorescent probes,[16–18] and optoelectronic devices.[19–25] There are two main approaches to their synthesis[26] (Scheme 1a): elimination of small molecule(s) such as carbon monoxide (CO) from precursors[27–30] and nucleophilic addition to quinones followed by reductive aromatization.[31,32] However, several problems may arise regarding the solubility and stability of the reaction intermediate with an increase in *n*.

In addition, [*n*]acenes have been reported to show switching behavior based on dynamic interconversion through photo- and thermal dimerization/dissociation and reversible endoperoxidation reaction.[33–39] For example, pentacene derivatives are interconvertible with their dimers, where the anthracene skeleton and/or naphthalene skeleton are unselectively formed by partial dearomatization. While these switching behaviors are fascinating from the viewpoint of control of HOMO/LUMO levels arising from the change in acene units, it is still challenging to attain reversible and selective switching of [*n*]acene units that can be observed in a unimolecular fashion rather than as an intermolecular reaction of two molecules.

Scheme 1. Synthetic procedures for acene derivatives. (a) Previous examples and (b) and (c) our strategies.

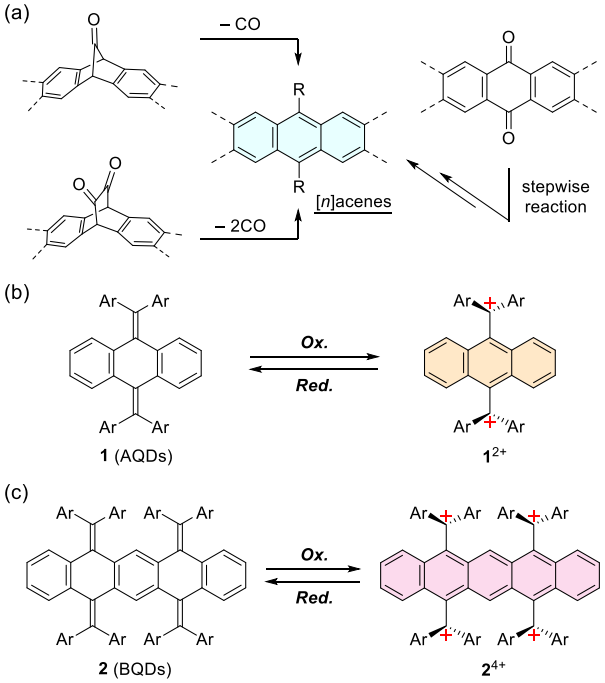

On the other hand, we recently reported that 11,11,12,12-tetraaryl-9,10-anthraquinodimethanes (AQDs) **1** with a folded form undergo one-stage two-electron oxidation to produce twisted dications with a planar anthracene skeleton (Scheme 1b).[40–42] These results

indicate that a [3]acene unit can be reversibly constructed by a redox reaction, accompanied by changes in both the structure and color of the molecule. Thus, we envisaged that extended [*n*]acenes could be formed in oligocationic states by one-stage oxidation of an accumulated structure composed of multiple AQD units, for instance, pentacene derivative would be obtained by four-electron oxidation of bisquinodimethane (BQD) **2** with eight aryl groups (Scheme 1c). In general, many extended [*n*]acenes are unstable due to the reactivity at the edges such as dimerization. However, this molecule $\mathbf{2}^{4+}$ is expected to be sufficiently stable because its highly reactive edges are protected by almost orthogonally twisted diarylmethylium units.

Herein, we propose a new approach for preparing extended [*n*]acenes by electrochemical oxidation, and demonstrate unprecedented hysteretic three-state redox interconversion among neutral BQDs **2**, tetracationic pentacenes $\mathbf{2}^{4+}$, and dicationic anthracenes $\mathbf{2}^{2+}$, in which both cations exhibit significantly red-shifted absorptions in the near-infrared (NIR) region based on an intramolecular charge-transfer (CT) interaction. Furthermore, all compounds in the neutral and cationic states were successfully isolated and demonstrated by single-crystal X-ray analyses, not only for electron-donating **2a** with methoxy groups, but also for pure hydrocarbon **2b** with *t*-butyl groups. The unimolecular redox switching behavior was characterized by spectroscopic and theoretical studies.

As shown in Figure 1a, the target molecules **2a** and **2b** were prepared from 5,7,12,14-pentacenetetrone over 4 steps, where stepwise introduction of aryl groups was conducted by Suzuki-Miyaura cross-coupling reaction following dibromoolefination. According to X-ray analyses, these BQDs with three non-fused benzene rings **2a** and **2b** adopt a zigzag conformation as shown in Figure 1b,c. By treatment with four equivalents of $(4\text{-}BrC_6H_4)_3N^{+\bullet}SbCl_6^-$ (Magic Blue), tetracationic salts $\mathbf{2a}^{4+}(SbCl_6^-)_4$ and $\mathbf{2b}^{4+}(SbCl_6^-)_4$ were isolated in 100% and 96% yields, respectively. X-ray analyses revealed that the tetracations have a fully conjugated planar pentacene core, which is almost orthogonal to the diarylmethylium moieties (Figure 1d,e); there are only a few examples of the determination of the structure of oligocations in organic molecules,[43–45] especially pure hydrocarbons.[46] The original BQDs **2a** and **2b** were completely recovered when tetracations were treated with an excess amount of Zn powder, which demonstrates that reversible redox interconversion between $\mathbf{2}/\mathbf{2}^{4+}$ can proceed. Both solid-state structures of BQDs **2** and tetracations $\mathbf{2}^{4+}$ were very similar to the geometries obtained by density functional theory (DFT) calculations at the CAM-B3LYP/6-31G* level (Figures S14-S17 and Tables S1-S3).

When the absorption spectra were measured in CH_2Cl_2 (Figure 2), tetracations $\mathbf{2}^{4+}$ exhibited strong absorptions in the visible region characteristic to diarylmethylium units [λ_{max}/nm (log ε): 517 (5.30) for $\mathbf{2a}^{4+}$ and 498 (5.08) for $\mathbf{2b}^{4+}$] as well as intramolecular CT absorptions in the NIR region [λ_{max}/nm (log ε): 922 (4.06) for $\mathbf{2a}^{4+}$ and 1094 (4.11) for $\mathbf{2b}^{4+}$], whereas BQDs **2** have absorption maxima only in the UV region [λ_{max}/nm (log ε): 328 (4.60) for **2a** and 317 (4.59) for **2b**]. A large red shift and vivid color change were observed upon four-electron oxidation of **2**.

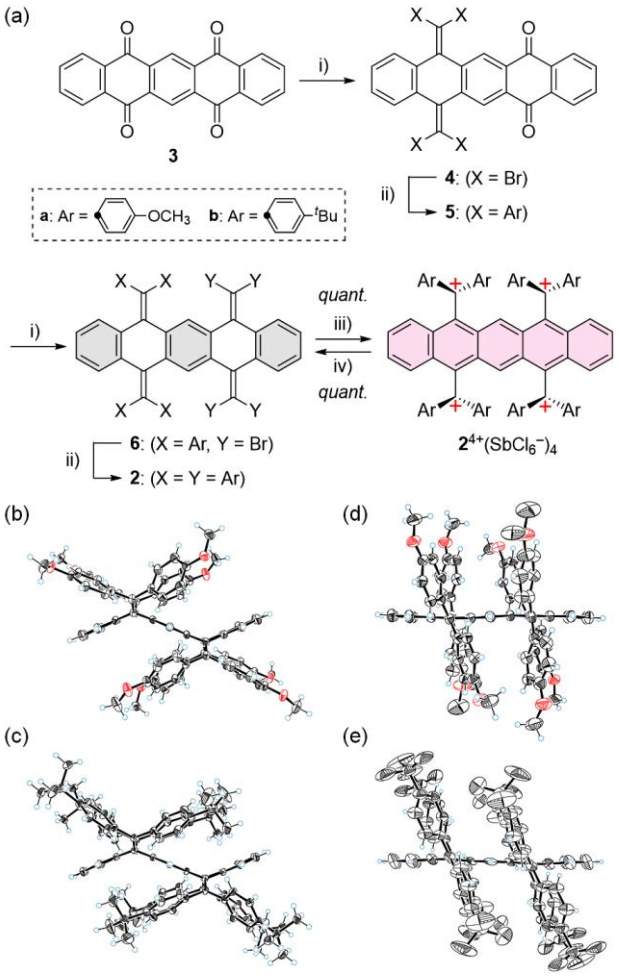

Figure 1. (a) Preparation of newly designed BQDs **2** and redox interconversion between **2** and $\mathbf{2}^{4+}$. i) CBr_4 and PPh_3 in toluene, ii) $ArB(OH)_2$ or $(ArBO)_3$, K_2CO_3, and $Pd(PPh_3)_4$ in toluene:EtOH:H_2O (10:1:1), iii) $(4\text{-}BrC_6H_4)_3N^{+\bullet}SbCl_6^-$ (4.0 eq) in CH_2Cl_2, and iv) Zn (excess) in CH_3CN. ORTEP drawings of (b) **2a**, (c) **2b**, (d) $\mathbf{2a}^{4+}(SbCl_6^-)_4$, and (e) $\mathbf{2b}^{4+}(SbCl_6^-)_4$. The counterions and solvent molecules are omitted for clarity. Thermal ellipsoids are shown at the 50% and 30% [only for $\mathbf{2b}^{4+}(SbCl_6^-)_4$] probability levels.

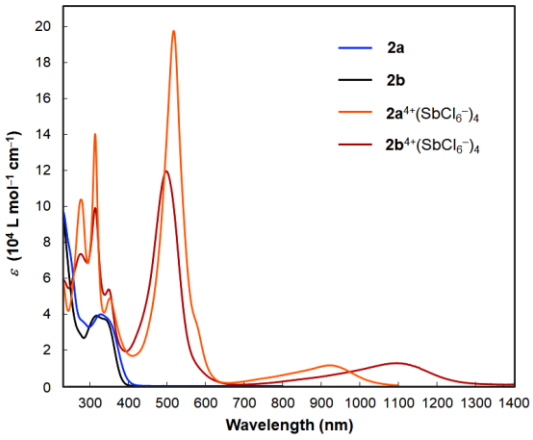

Figure 2. UV–vis–NIR spectra of **2a** (blue), **2b** (black), $\mathbf{2a}^{4+}(SbCl_6^-)_4$ (orange), and $\mathbf{2b}^{4+}(SbCl_6^-)_4$ (red) in CH_2Cl_2.

Each absorption band was assigned by time-dependent (TD)-DFT calculations (Figure S24a,b). Note that the pure hydrocarbon $\mathbf{2b}^{4+}$ shows significantly red-shifted CT absorptions, which can be accounted for by a low-lying LUMO level due to the lower donating ability of *t*-butyl groups for $\mathbf{2b}^{4+}$ than methoxy groups for $\mathbf{2a}^{4+}$, while the coefficients in HOMO are located on the same pentacene core. The lower-energy CT bands for tetracationic pentacenes $\mathbf{2}^{4+}$ compared to dicationic anthracenes $\mathbf{1}^{2+}$ [λ_{max}/nm (log ε): 709 (3.94) for $\mathbf{1a}^{2+}$ and 836 (3.95) for $\mathbf{1b}^{2+}$] can be explained by the higher donating ability of pentacene compared to the anthracene core (Figures S22-S24).

To investigate the redox properties in detail, we conducted cyclic voltammetry in CH_2Cl_2 (Figure 3a). For **2a**, the voltammogram showed a one-wave four-electron oxidation peak at +1.12 V (vs. SCE), which is close to that of **1a** (+1.03 V) (Figure S25).[40] The one-stage four-electron process for oxidation was verified by using ferrocene as an external standard and confirmed by differential pulse voltammetry (Figure S28). As a result of the change in structures, return peaks, where two-stage two-electron reduction occurs via intermediate dication $\mathbf{2a}^{2+}$, appeared in the far cathodic region (E^{red}/V: +0.55 for $\mathbf{2a}^{4+}$ and +0.27 for $\mathbf{2a}^{2+}$). Such a cathodic peak shift is a characteristic feature of dynamic redox (*dyrex*) systems,[47] in which the steady-state concentration of intermediate radical species ($\mathbf{2a}^{+\bullet}$ or $\mathbf{2a}^{3+\bullet}$) is negligible. The smaller current of the return peaks is due to the effects of diffusion. Similar redox behavior was observed for **2b** (E^{ox}/V: +1.26 for **2b**; E^{red}/V: +0.89 for $\mathbf{2b}^{4+}$ and +0.76 for $\mathbf{2b}^{2+}$).

According to these observations, three structures can be considered as the intermediary dication $\mathbf{2}^{2+}$: (A) dication diradical with a pentacene skeleton as in $\mathbf{2}^{4+}$, (B) diagonally conjugated quinoidal dication, and (C) localized dication with an anthracene skeleton fused with an AQD unit. They all have some advantages: there would be highly delocalized cations and radicals in A, less Coulombic repulsion in B, and intramolecular CT interaction in C. We first investigated if these dications $\mathbf{2}^{2+}$ are diradical species having a pentacene core via voltammetric analyses by immediately reoxidizing the as-prepared dicationic species that were generated at the first two-electron reduction peak (Figure S26). There was no corresponding oxidation peak in either $\mathbf{2a}^{2+}$ or $\mathbf{2b}^{2+}$, meaning that a significant structural change rapidly occurs in $\mathbf{2}^{2+}$ to lose the pentacene structure when the tetracations are reduced, so that the possibility of diradical species (A) could be excluded.

To obtain further information regarding the structure of the intermediary dications $\mathbf{2}^{2+}$ as expected by the voltammetric analyses of BQDs **2**, we performed a titration experiment on the chemical reduction of $\mathbf{2}^{4+}$, which was monitored by UV–vis–NIR spectroscopy. Upon the addition of aliquots of Bu_4NI (TBAI) in CH_2Cl_2, the UV–vis–NIR spectrum of $\mathbf{2b}^{4+}$ changed to that of **2b** via the intermediate dication $\mathbf{2b}^{2+}$ in a stepwise fashion, where several isosbestic points were observed in both stages. Especially in the first stage, the absorption maxima at 498 and 1094 nm for $\mathbf{2b}^{4+}$ in the visible and NIR region shifted to 509 and 1005 nm for $\mathbf{2b}^{2+}$ (Figure 3b). Similar results were obtained by using $\mathbf{2a}^{4+}$ with decamethylferrocene [$(CH_3)_{10}Fc$] (Figure S30). The NIR absorption of dications $\mathbf{2}^{2+}$ suggested that the C form with intramolecular CT interaction would be likely, and this idea is supported by the fact that the DFT method gave no energy-minimized structure for the quinoidal B form. At the same time, titration experiments indicated that the intermediary dications $\mathbf{2}^{2+}$ have a long lifetime as observed by spectroscopic measurements and do not disproportionate into neutral BQDs **2** and tetracations $\mathbf{2}^{4+}$.

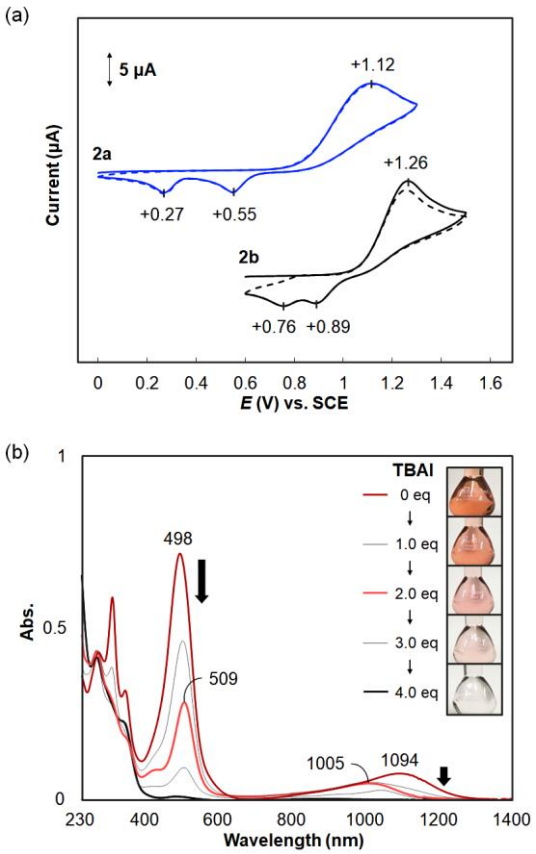

Figure 3. (a) Cyclic voltammograms of **2a** and **2b** at 297 K in CH_2Cl_2 containing 0.1 M Bu_4NBF_4 as a supporting electrolyte (scan rate 0.1 V s^{-1}, Pt electrodes). The second cycles are shown by a dashed line. (b) Change in UV–vis–NIR spectrum of $\mathbf{2b}^{4+}(SbCl_6^-)_4$ (6.00 μM) upon the addition of several aliquots of TBAI in CH_2Cl_2.

After many trials, dications $\mathbf{2}^{2+}$ could be isolated in pure form. Upon two-electron reduction of tetracationic salts $\mathbf{2a}^{4+}(SbCl_6^-)_4$ and $\mathbf{2b}^{4+}(SbCl_6^-)_4$ in CH_3CN with two equivalents of $(CH_3)_{10}Fc$ and TBAI, respectively, dicationic salts $\mathbf{2a}^{2+}(SbCl_6^-)_2$ and $\mathbf{2b}^{2+}(SbCl_6^-)_2$ were isolated in 99% and 95% yields, respectively (Figure 4a). These structures of dications $\mathbf{2}^{2+}$ are C forms, consisting of bis(diarylmethylium)-substituted anthracene and a tetraarylquinodimethane unit, as characterized by ^1H NMR spectra and finally determined by single-crystal X-ray analyses, as shown in Figure 4b,c. Since their NIR absorption bands are assigned to the intramolecular CT interaction between electron-accepting cationic moieties and electron-donating diarylmethylene units by TD-DFT calculations at the CAM-B3LYP/6-31G* level (Figure S24c,d), the structures in solution are considered to be the same as those in crystals. We also confirmed that the CT absorption bands (794 nm for $\mathbf{2a}^{2+}$ and 1000 nm for $\mathbf{2b}^{2+}$) were ob-

served at a longer-wavelength region than those for $\mathbf{1}^{2+}$ (709 nm for $\mathbf{1a}^{2+}$ and 836 nm for $\mathbf{1b}^{2+}$), which exhibits CT interaction between cationic moieties as an acceptor and anthracene skeleton as a donor (Figure S29).

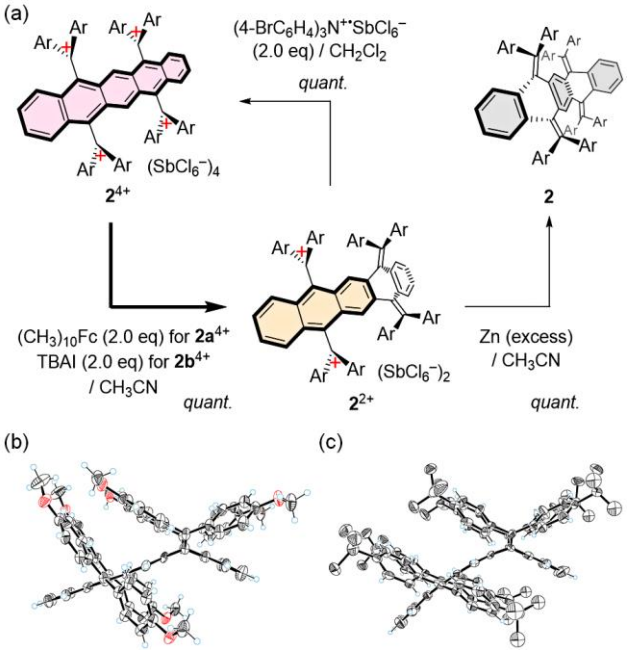

Figure 4. (a) Isolation of dications $\mathbf{2a}^{2+}(SbCl_6^-)_2$ and $\mathbf{2b}^{2+}(SbCl_6^-)_2$ and redox interconversion among $\mathbf{2}^{2+}$ and $\mathbf{2}/\mathbf{2}^{4+}$. ORTEP drawings of (b) $\mathbf{2a}^{2+}(SbCl_6^-)_2$ and (c) $\mathbf{2b}^{2+}(SbCl_6^-)_2$. The counterions and solvent molecules are omitted for clarity. Thermal ellipsoids are shown at the 50% and 30% probability levels, respectively.

Variable-temperature ^{1}H NMR measurement revealed that there is very slow intramolecular electron-transfer because we cannot observe any broadening or coalescence of NMR signals of $\mathbf{2a}^{2+}(SbCl_6^-)_2$ in CD_3CN (Figure S31). Thus, each redox part behaves independently, and voltammetric analyses of $\mathbf{2}^{2+}$ show that one-stage two-electron oxidation of the AQD unit occurred at +0.95 V for $\mathbf{2a}^{2+}$ and +1.26 V for $\mathbf{2b}^{2+}$, and one-stage two-electron reduction peaks of dicationic anthracene were observed at +0.20 V for $\mathbf{2a}^{2+}$ and +0.73 V for $\mathbf{2b}^{2+}$ (Figure S27). Actually, when dications $\mathbf{2}^{2+}$ were treated with two equivalents of Magic Blue and with an excess amount of Zn powder, tetracations $\mathbf{2}^{4+}$ and BQDs **2** were isolated quantitatively for both reactions. Therefore, unprecedented hysteretic three-state redox interconversion among tetracationic pentacenes $\mathbf{2}^{4+}$, dicationic anthracenes $\mathbf{2}^{2+}$, and neutral BQDs **2**, as shown by cyclic voltammetry, was demonstrated on a preparative scale.

With the exact structure and detailed redox properties of dications $\mathbf{2}^{2+}$ in hand, we can now explain why BQDs **2** undergo one-stage four-electron oxidation. The HOMOs of **2** have coefficients on the atoms in both AQD units, and thus two-electron oxidation of **2** does not occur to form dications $\mathbf{2}^{2+}$ of C form (Figures S18-S19). Furthermore, based on the similar oxidation potentials of $\mathbf{2}^{2+}$ and **2**, we can rule out the possibility that orthogonally attached cationic units cause on-site Coulombic repulsion to retard multiple-electron transfer.

In conclusion, we designed and synthesized zigzag-structured BQD derivatives **2** with non-fused benzene rings, which undergo one-stage four-electron oxidation to produce tetracationic pentacene derivatives $\mathbf{2}^{4+}$ with a doubly twisted conformation. When tetracationic pentacenes $\mathbf{2}^{4+}$ were reduced, two-stage two-electron reduction occurs via dicationic anthracenes $\mathbf{2}^{2+}$ to the original BQDs **2**. Such hysteretic three-state redox interconversion among them demonstrates perfect control of the number of fused benzene rings ([1] -> [5] -> [3] -> [1]) in the [*n*]acene structure by redox conversion. It is noteworthy that cationic species can be isolated even for pure hydrocarbons. Furthermore, since these cations exhibit significantly red-shifted NIR absorptions (-1,400 nm) based on intramolecular CT interaction, changes in structure as well as UV–vis–NIR absorptions can be controlled by redox switching. These results provide a new tactic for creating [*n*]acene-based redox switches with fully controlled multiple-electron transfer, and for dynamically interconverting their structures and properties in a unimolecular fashion.

ASSOCIATED CONTENT

Supporting Information.
The Supporting Information is available free of charge via the Internet at http://pubs.acs.org.
Synthetic details, characterization data, theoretical study, spectra, and crystallographic details (PDF)
X-ray crystallographic data (CIF)

AUTHOR INFORMATION

Corresponding Author

*yishigaki@sci.hokudai.ac.jp
*tak@sci.hokudai.ac.jp

ORCID

Yusuke Ishigaki: 0000-0001-7961-3595
Takanori Suzuki: 0000-0002-1230-2044

Notes

The authors declare no competing financial interest.

ACKNOWLEDGMENT

This work was supported by JSPS KAKENHI Grant Numbers JP19K15528, JP20H02719, and JP20K21184. Y.I. acknowledges Toyota Riken Scholar, The NOVARTIS Foundation, and The Hattori Hokokai Foundation for the Promotion of Science.

REFERENCES

(1) Dang, H.; Garcia-Garibay, M. A. Palladium-Catalyzed Formation of Aceanthrylenes: A Simple Method for Peri-Cyclopentenelation of Aromatic Compounds. *J. Am. Chem. Soc.* **2001**, *123*, 355–356.
(2) Anthony, J. E.; Brooks, J. S.; Eaton, D. L.; Parkin, S. R. Functionalized Pentacene: Improved Electronic Properties from Control of Solid-State Order. *J. Am. Chem. Soc.* **2001**, *123*, 9482–9483.
(3) Sakamoto, Y.; Suzuki, T.; Kobayashi, M.; Gao, Y.; Fukai, Y.; Inoue, Y.; Sato, F.; Tokito, S. Perfluoropentacene: High-Performance p–n Junctions and Complementary Circuits with Pentacene. *J. Am. Chem. Soc.* **2004**, *126*, 8138–8140.

(4) Payne, M. M.; Parkin, S. R.; Anthony, J. E. Functionalized Higher Acenes: Hexacene and Heptacene. *J. Am. Chem. Soc.* **2005**, *127*, 8028–8029.
(5) Purushotham, U.; Sastry, G. N. Conjugate Acene Fused Buckybowls: Evaluating Their Suitability for p-Type, Ambipolar and n-Type Air Stable Organic Semiconductors. *Phys. Chem. Chem. Phys.* **2013**, *15*, 5039–5048.
(6) Naibi Lakshminarayana, A.; Chang, J.; Luo, J.; Zheng, B.; Huang, K.-W.; Chi, C. Bisindeno-Annulated Pentacenes with Exceptionally High Photo-Stability and Ordered Molecular Packing: Simple Synthesis by a Regio-Selective Scholl Reaction. *Chem. Commun.* **2015**, *51*, 3604–3607.
(7) Bheemireddy, S. R.; Ubaldo, P. C.; Rose, P. W.; Finke, A. D.; Zhuang, J.; Wang, L.; Plunkett, K. N. Stabilizing Pentacene By Cyclopentannulation. *Angew. Chem. Int. Ed.* **2015**, *54*, 15762–15766.
(8) Hu, Y.; Thomas, M. B.; Webre, W. A.; Moss, A.; Jinadasa, R. G. W.; Nesterov, V. N.; D'Souza, F.; Wang, H. Nickel(II) Bisporphyrin-Fused Pentacenes Exhibiting Abnormal High Stability. *Angew. Chem. Int. Ed.* **2020**, *59*, 20075–20082.
(9) Pascal, R. A. Twisted Acenes. *Chem. Rev.* **2006**, *106*, 4809–4819.
(10) Clevenger, R. G.; Kumar, B.; Menuey, E. M.; Kilway, K. V. Synthesis and Structure of a Longitudinally Twisted Hexacene. *Chem. Eur. J.* **2018**, *24*, 3113–3116.
(11) Bedi, A.; Shimon, L. J. W.; Gidron, O. Helically Locked Tethered Twistacenes. *J. Am. Chem. Soc.* **2018**, *140*, 8086–8090.
(12) Anthony, J. E. Functionalized Acenes and Heteroacenes for Organic Electronics. *Chem. Rev.* **2006**, *106*, 5028–5048.
(13) Pilevarshahri, R.; Rungger, I.; Archer, T.; Sanvito, S.; Shahtahmassebi, N. Spin Transport in Higher *n*-Acene Molecules. *Phys. Rev. B* **2011**, *84*, 174437.
(14) Paulus, F.; Engelhart, J. U.; Hopkinson, P. E.; Schimpf, C.; Leineweber, A.; Sirringhaus, H.; Vaynzof, Y.; Bunz, U. H. F. The Effect of Tuning the Microstructure of TIPS-Tetraazapentacene on the Performance of Solution Processed Thin Film Transistors. *J. Mater. Chem. C* **2016**, *4*, 1194–1200.
(15) Pham, H. D.; Hu, H.; Wong, F.-L.; Lee, C.-S.; Chen, W.-C.; Feron, K.; Manzhos, S.; Wang, H.; Motta, N.; Lam, Y. M.; Sonar, P. Acene-Based Organic Semiconductors for Organic Light-Emitting Diodes and Perovskite Solar Cells. *J. Mater. Chem. C* **2018**, *6*, 9017–9029.
(16) Brega, V.; Yan, Y.; Thomas, S. W. Acenes beyond Organic Electronics: Sensing of Singlet Oxygen and Stimuli-Responsive Materials. *Org. Biomol. Chem.* **2020**, *18*, 9191–9209.
(17) McDaniel, D. K.; Jo, A.; Ringel-Scaia, V. M.; Coutermarsh-Ott, S.; Rothschild, D. E.; Powell, M. D.; Zhang, R.; Long, T. E.; Oestreich, K. J.; Riffle, J. S.; Davis, R. M.; Allen, I. C. TIPS Pentacene Loaded PEO-PDLLA Core-Shell Nanoparticles Have Similar Cellular Uptake Dynamics in M1 and M2 Macrophages and in Corresponding *in vivo* Microenvironments. *Nanomed. Nanotechno.* **2017**, *13*, 1255–1266.
(18) Uchiyama, Y.; Watanabe, R.; Kurotaki, T.; Kuniya, S.; Kimura, S.; Sawamura, Y.; Ohtsuki, T.; Kikuchi, Y.; Matsuzawa, H.; Uchiyama, K.; Itakura, M.; Kawakami, F.; Maruyama, H. Maintaining of the Green Fluorescence Emission of 9-Aminoanthracene for Bioimaging Applications. *ACS Omega* **2017**, *2*, 3371–3379.
(19) Wilson, M. W. B.; Rao, A.; Johnson, K.; Gélinas, S.; di Pietro, R.; Clark, J.; Friend, R. H. Temperature-Independent Singlet Exciton Fission in Tetracene. *J. Am. Chem. Soc.* **2013**, *135*, 16680–16688.
(20) Basel, B. S.; Hetzer, C.; Zirzlmeier, J.; Thiel, D.; Guldi, R.; Hampel, F.; Kahnt, A.; Clark, T.; Guldi, D. M.; Tykwinski, R. R. Davydov Splitting and Singlet Fission in Excitonically Coupled Pentacene Dimers. *Chem. Sci.* **2019**, *10*, 3854–3863.
(21) Yablon, L. M.; Sanders, S. N.; Li, H.; Parenti, K. R.; Kumarasamy, E.; Fallon, K. J.; Hore, M. J. A.; Cacciuto, A.; Sfeir, M. Y.; Campos, L. M. Persistent Multiexcitons from Polymers with Pendent Pentacenes. *J. Am. Chem. Soc.* **2019**, *141*, 9564–9569.
(22) Papadopoulos, I.; Gao, Y.; Hetzer, C.; Tykwinski, R. R.; Guldi, D. M. Singlet Fission in Enantiomerically Pure Pentacene Dimers. *ChemPhotoChem* **2020**, *4*, 5168–5174.
(23) Lijina, M. P.; Benny, A.; Ramakrishnan, R.; Nair, N. G.; Hariharan, M. Exciton Isolation in Cross-Pentacene Architecture. *J. Am. Chem. Soc.* **2020**, *142*, 17393–17402.
(24) Fallon, K. J.; Churchill, E. M.; Sanders, S. N.; Shee, J.; Weber, J. L.; Meir, R.; Jockusch, S.; Reichman, D. R.; Sfeir, M. Y.; Congreve, D. N.; Campos, L. M. Molecular Engineering of Chromophores to Enable Triplet–Triplet Annihilation Upconversion. *J. Am. Chem. Soc.* **2020**, *142*, 19917–19925.
(25) Bergman, H. M.; Kiel, G. R.; Witzke, R. J.; Nenon, D. P.; Schwartzberg, A. M.; Liu, Y.; Tilley, T. D. Shape-Selective Synthesis of Pentacene Macrocycles and the Effect of Geometry on Singlet Fission. *J. Am. Chem. Soc.* **2020**, *142*, 19850–19855.
(26) Dorel, R.; Echavarren, A. M. Strategies for the Synthesis of Higher Acenes. *Eur. J. Org. Chem.* **2017**, *2017*, 14–24.
(27) Chen, K.-Y.; Hsieh, H.-H.; Wu, C.-C.; Hwang, J.-J.; Chow, T. J. A New Type of Soluble Pentacene Precursor for Organic Thin-Film Transistors. *Chem. Commun.* **2007**, 1065–1067.
(28) Watanabe, M.; Chang, Y. J.; Liu, S.-W.; Chao, T.-H.; Goto, K.; Islam, M. M.; Yuan, C.-H.; Tao, Y.-T.; Shinmyozu, T.; Chow, T. J. The Synthesis, Crystal Structure and Charge-Transport Properties of Hexacene. *Nat. Chem.* **2012**, *4*, 574–578.
(29) Hayashi, H.; Hieda, N.; Yamauchi, M.; Chan, Y. S.; Aratani, N.; Masuo, S.; Yamada, H. Visible‐Light‐Induced Heptacene Generation under Ambient Conditions: Utilization of Single‐crystal Interior as an Isolated Reaction Site. *Chem. Eur. J.* **2020**, *26*, 15079–15083.
(30) Yamada, H.; Kuzuhara, D.; Suzuki, M.; Hayashi, H.; Aratani, N. Synthesis and Morphological Control of Organic Semiconducting Materials Using the Precursor Approach. *Bull. Chem. Soc. Jpn.* **2020**, *93*, 1234–1267.
(31) Kaur, I.; Jazdzyk, M.; Stein, N. N.; Prusevich, P.; Miller, G. P. Design, Synthesis, and Characterization of a Persistent Nonacene Derivative. *J. Am. Chem. Soc.* **2010**, *132*, 1261–1263.
(32) Tykwinski, R. R. Synthesis of Unsymmetrical Derivatives of Pentacene for Materials Applications. *Acc. Chem. Res.* **2019**, *52*, 2056–2069.
(33) Berg, O.; Chronister, E. L.; Yamashita, T.; Scott, G. W.; Sweet, R. M.; Calabrese, J. *s*-Dipentacene: Structure, Spectroscopy, and Temperature- and Pressure-Dependent Photochemistry. *J. Phys. Chem. A* **1999**, *103*, 2451–2459.
(34) Zade, S. S.; Zamoshchik, N.; Reddy, A. R.; Fridman-Marueli, G.; Sheberla, D.; Bendikov, M. Products and Mechanism of Acene Dimerization. A Computational Study. *J. Am. Chem. Soc.* **2011**, *133*, 10803–10816.
(35) Einholz, R.; Fang, T.; Berger, R.; Grüninger, P.; Früh, A.; Chassé, T.; Fink, R. F.; Bettinger, H. F. Heptacene: Characterization in Solution, in the Solid State, and in Films. *J. Am. Chem. Soc.* **2017**, *139*, 4435–4442.
(36) Dong, S.; Ong, A.; Chi, C. Photochemistry of Various Acene Based Molecules. *J. Photochem. Photobiol. C Photochem. Rev.* **2019**, *38*, 27–46.
(37) Fudickar, W.; Linker, T. Why Triple Bonds Protect Acenes from Oxidation and Decomposition. *J. Am. Chem. Soc.* **2012**, *134*, 15071–15082.
(38) Gao, Z.; Han, Y.; Wang, F. Cooperative Supramolecular Polymers with Anthracene–endoperoxide Photo-Switching for Fluorescent Anti-Counterfeiting. *Nat. Commun.* **2018**, *9*, 3977.
(39) Liu, K.; Lalancette, R. A.; Jäkle, F. Tuning the Structure and Electronic Properties of B–N Fused Dipyridylanthracene and Implications on the Self-Sensitized Reactivity with Singlet Oxygen. *J. Am. Chem. Soc.* **2019**, *141*, 7453–7462.

(40) Ishigaki, Y.; Sugawara, K.; Yoshida, M.; Kato, M.; Suzuki, T. Two-Way Chromic Systems Based on Tetraarylanthraquinodimethanes: Electrochromism in Solution and Mechanofluorochromism in a Solid State. *Bull. Chem. Soc. Jpn.* **2019**, *92*, 1211–1217.
(41) Ishigaki, Y.; Hayashi, Y.; Suzuki, T. Photo- and Thermal Interconversion of Multiconfigurational Strained Hydrocarbons Exhibiting Completely Switchable Oxidation to Stable Dicationic Dyes. *J. Am. Chem. Soc.* **2019**, *141*, 18293–18300.
(42) Ishigaki, Y.; Hashimoto, T.; Sugawara, K.; Suzuki, S.; Suzuki, T. Switching of Redox Properties Triggered by a Thermal Equilibrium between Closed-Shell Folded and Open-Shell Twisted Species. *Angew. Chem. Int. Ed.* **2020**, *59*, 6581–6584.
(43) Sakamaki, D.; Ito, A.; Tsutsui, Y.; Seki, S. Tetraaza[1_4]- and Octaaza[1_8]Paracyclophane: Synthesis and Characterization of Their Neutral and Cationic States. *J. Org. Chem.* **2017**, *82*, 13348–13358.
(44) Nguyen, M. T.; Ferris, D. P.; Pezzato, C.; Wang, Y.; Stoddart, J. F. Densely Charged Dodecacationic [3]- and Tetracosacationic Radial [5]Catenanes. *Chem* **2018**, *4*, 2329–2344.
(45) Ni, Y.; Gopalakrishna, T. Y.; Phan, H.; Kim, T.; Herng, T. S.; Han, Y.; Tao, T.; Ding, J.; Kim, D.; Wu, J. 3D Global Aromaticity in a Fully Conjugated Diradicaloid Cage at Different Oxidation States. *Nat. Chem.* **2020**, *12*, 242–248.
(46) Ni, Y.; Gordillo-Gámez, F.; Peña Alvarez, M.; Nan, Z.; Li, Z.; Wu, S.; Han, Y.; Casado, J.; Wu, J. A Chichibabin's Hydrocarbon-Based Molecular Cage: The Impact of Structural Rigidity on Dynamics, Stability, and Electronic Properties. *J. Am. Chem. Soc.* **2020**, *142*, 12730–12742.
(47) Suzuki, T.; Tamaoki, H.; Nishida, J.; Higuchi, H.; Iwai, T.; Ishigaki, Y.; Hanada, K.; Katoono, R.; Kawai, H.; Fujiwara, K.; Fukushima, T. Redox-Mediated Reversible σ-Bond Formation/Cleavage. In *Organic Redox Systems*; Wiley, Hoboken, NJ, **2015**, pp 13–37.

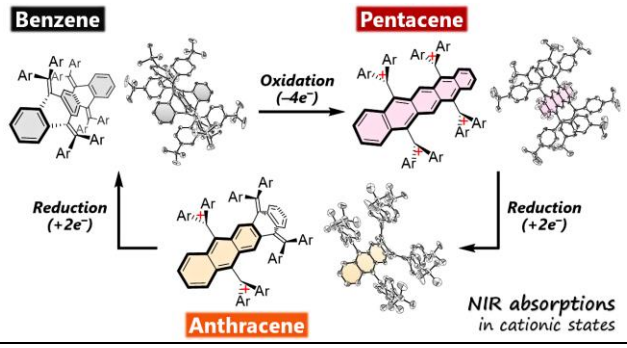
Benzene
Pentacene
Oxidation
(–4e⁻)
Reduction
(+2e⁻)
Reduction
(+2e⁻)
Anthracene
NIR absorptions
in cationic states